Shallow traps and radiative recombination processes in $Lu_3Al_5O_{12}$:Ce single crystal scintillator

M. Nikl,[1,2] A. Vedda,[1] M. Fasoli,[1] I. Fontana,[1] V. V. Laguta,[2] E. Mihokova,[2] J. Pejchal,[2] J. Rosa,[2] and K. Nejezchleb[3]
[1]*Dipartimento di Scienza dei Materiali dell' Universita di Milano "Bicocca," Via Cozzi 53, 20 125 Milano, Italy*
[2]*Institute of Physics AS CR, Cukrovarnicka 10, 162 53 Prague, Czech Republic*
[3]*CRYTUR Ltd., Palackeho 175, 511 19 Turnov, Czech Republic*
(Received 31 July 2007; published 21 November 2007)

Thermally stimulated luminescence (TSL) glow curves and emission spectra were studied in undoped and Ce-doped $Lu_3Al_5O_{12}$ single crystals by wavelength resolved TSL measurements in the 10–310 K temperature range. Isothermal phosphorescence measurements in the 10–100 K range were also performed, which point to the existence of a tunneling-driven radiative recombination process. These processes can explain the presence and time-dependence of the submicrosecond slow decay component in the scintillation decay. Electron paramagnetic resonance experiments suggest the presence of Lu_{Al} defects in the vicinity of Ce^{3+} ions, which are the most probable electron and hole traps participating in the tunneling-driven radiative recombination process.

DOI: 10.1103/PhysRevB.76.195121 PACS number(s): 78.60.Kn, 78.47.+p, 78.66.Nk

I. INTRODUCTION

$Y_3Al_5O_{12}$ (YAG) single crystals were among the first oxide materials grown by the Czochralski technique in the 1960s.[1] Their development was stimulated mainly by the application for solid state lasers (Nd^{3+} doped), but soon the potential of Ce^{3+}-doped YAG as a fast scintillator was recognized too.[2] The first comprehensive description of YAG:Ce scintillator characteristics was reported by Moszynski *et al.*,[3] who included this material among the high figure-of-merit oxide scintillators. Isostructural $Lu_3Al_5O_{12}$ (LuAG) has a higher density (6.67 g/cm^3) with respect to YAG (4.56 g/cm^3), which is an advantage in the case of hard x- and gamma-ray detection. LuAG:Ce scintillator became of interest relatively recently.[4–6] In both Ce-doped YAG and LuAG single crystals grown from high temperature melt (Czochralski, Bridgman, or similar techniques), very slow decay processes in the scintillation response were detected.[7] Their presence explains the fact that their light yield within 1 μs time gate is only about 300% and 150% of $Bi_4Ge_3O_{12}$ (BGO),[8] even if their scintillation efficiency (integral of radio-luminescence spectra) is similar and reaches about 700% of BGO at room temperature.[7] Such slow components usually arise due to retrapping of free charge carriers at shallow traps, which delay their radiative recombination with holes trapped at Ce ions. Recent thermally stimulated luminescence (TSL) measurements revealed the presence of dominant shallow electron traps both in YAG:Ce (Ref. 9) and LuAG:Ce (Ref. 10) with thermal depths of about 0.18 and 0.29 eV, respectively. They were ascribed to antisite Y_{Al} and Lu_{Al} defects, i.e., Y and Lu ions residing at Al octahedral sites. Bondings of Y and Lu ions localized at octahedral Al sites feature a higher degree of covalency with respect to those in regular dodecahedral sites resulting in a low energy shift of their energy levels from the very bottom of the conduction band (see band structure calculations of YAG in Refs. 11 and 12) into the forbidden gap. Recent theoretical calculations[13,14] demonstrated that such defects are those with the highest occurrence probability in these garnet structures. Furthermore, "antisite" localization of Nd^{3+} and Er^{3+} rare earth ions at Al (Ga) octahedral sites has been evidenced by high resolution spectroscopy in aluminum (gallium) garnets.[15,16] The higher melting temperature and the smaller difference between Lu^{3+} and Al^{3+} radii might result in a higher concentration of antisite defect-related traps in LuAG host with respect to YAG; so, taking also into account their increased thermal depth, such defects might have a greater detrimental effect on the energy transfer to Ce^{3+} ions. This could explain the lower light yield of LuAG:Ce with respect to that of YAG:Ce.

Electron paramagnetic resonance (EPR) investigations performed on LuAG:Ce suggested the presence of Lu_{Al} antisite defects close to Ce^{3+} ions perturbing Ce^{3+} EPR signals.[17] Such nearby lying hole and electron traps might enable the tunneling recombination of charge carriers captured during irradiation. In fact, such process was evidenced in phosphorescence measurements in the 10–40 K temperature interval following x-ray irradiation,[7] as the decays appear temperature independent and follow a t^{-1} time dependence in the time scale from seconds to hours in accordance with the theoretical expectation.[18]

The aim of this paper is to deepen the TSL analysis below room temperature in undoped and Ce-doped LuAG single crystals. Based on this investigation, an interpretation of slower decay components observed in the scintillation response of this material is proposed. Supporting arguments from systematic EPR experiments are also provided.

II. EXPERIMENTAL CONDITIONS

Wavelength-resolved TSL measurements were performed in the 10–310 K range using a CTI closed-cycle refrigerator after x-ray irradiation at 10 K (with a Philips 2274 x-ray tube operated at 20 kV), with a homemade apparatus allowing the detection of the TSL signal both as a function of temperature and wavelength in the 280–710 nm interval. A heating rate of 0.1 K/s was adopted. Phosphorescence decays were measured by the same setup after x-ray irradiation at fixed temperature in the 10–100 K interval. Scintillation decays were measured at room temperature (RT) under ^{22}Na radioisotope excitation (511 keV photons) using the time-correlated single photon counting method by a modified Spectrofluo-

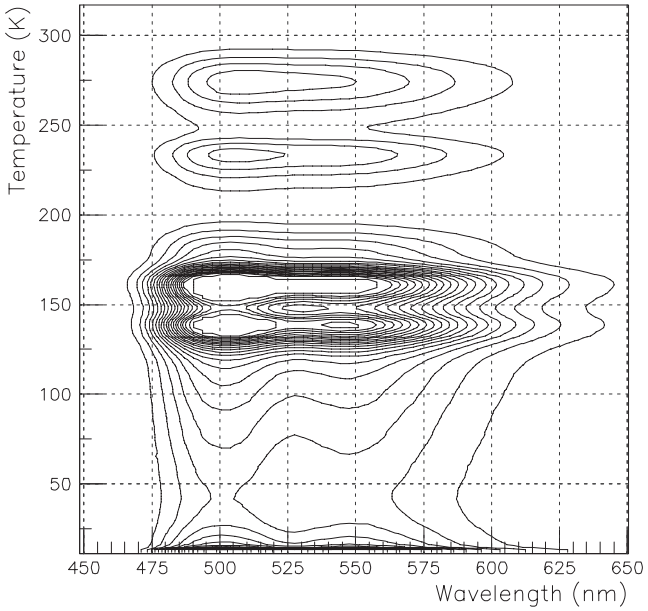

FIG. 1. Contour plot of a wavelength resolved TSL measurement performed on LuAG:0.07 wt % Ce after x-ray irradiation at 10 K. Heating rate=0.1 K/s.

rometer 199S (Edinburgh Instrument). EPR studies were performed at 9.22 GHz with the standard 3 cm wavelength of the EPR spectrometer; measurements were performed in the temperature range 4–300 K using an Oxford Instruments cryostat.

Single crystals with typical dimensions $\varnothing 20\times 50$ mm of three undoped (un1, un2, and un3) and three Ce-doped lutetium aluminum garnets (Ce concentrations in the crystals, 0.03, 0.07, and 0.12 wt %) were grown by the Czochralski technique from 4*N* Lu_2O_3, 4*N* Al_2O_3 (un1 and un2), and 5*N* Lu_2O_3 and 4*N* Al_2O_3 (the rest of samples) raw powders in a molybdenum crucible under reducing atmosphere by CRYTUR, Ltd. (Turnov, Czech Republic). Due to the reducing atmosphere of the growth, perfect linear dependence of the Ce^{3+} absorption band amplitude on the total Ce content in the crystal, and high steady-state scintillation efficiency of the Ce-doped samples,[7] the content of Ce^{4+} is supposed to be negligible, i.e., the concentration of Ce^{3+} should approach the numbers of total Ce concentration given above. Plates of about $7\times 7\times 1$ mm^3, cubes of about 1 cm^3, and oriented samples of about $2\times 2\times 6$ mm^3 were cut and polished for TSL, scintillation decay and EPR experiments, respectively. In addition, liquid phase epitaxy (LPE) grown LuAG:Ce films studied in Ref. 10 were also used for EPR experiments. These single crystalline films were grown on YAG substrates using the PbO-based flux. Their typical thickness was about 20 μm; for other details, see Ref. 10.

III. EXPERIMENTAL RESULTS

A. Thermally stimulated luminescence

An example of a wavelength resolved TSL measurement is displayed in Fig. 1 in the case of the sample doped with 0.07 wt % of cerium. The reported contour plot shows the

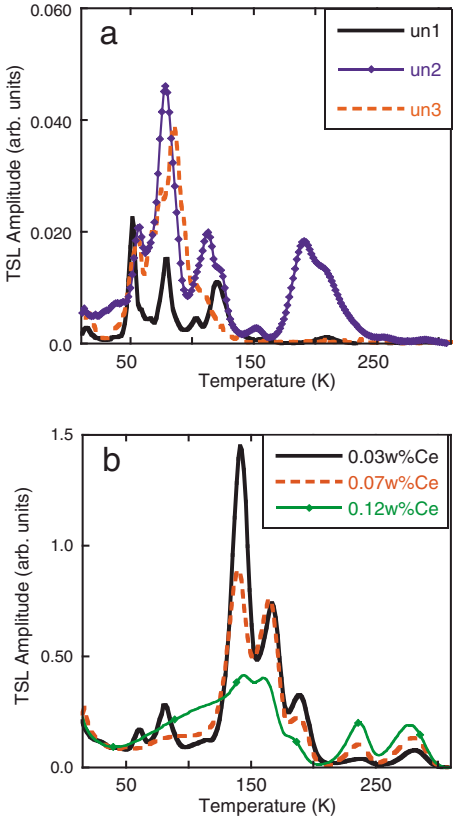

FIG. 2. (Color online) TSL glow curves after x-ray irradiation at 10 K for (a) undoped LuAG samples and (b) Ce-doped ones. X-ray dose=dose 10 Gy. All curves are mutually comparable in an absolute way.

emitted light both as a function of temperature and emission wavelength. After the integration of wavelength resolved measurements in the 280–710 and 460–660 nm wavelength intervals TSL glow curves of the undoped and Ce-doped samples were obtained, respectively, which are displayed in Figs. 2(a) and 2(b). A complete change of the TSL pattern due to Ce^{3+} doping can be noticed since peaks characteristic of undoped crystals in the 40–100 K interval are barely evident only in the sample with the lowest Ce concentration and completely disappear by increasing the cerium content. At variance, Ce-doped samples display the characteristic triple peak structure ascribed to electron traps associated with Lu_{Al} antisite defects in the 120–200 K range. Moreover, a broad structureless signal below 120 K strongly increases with the Ce concentration, while an opposite trend occurs for the 140 K peak. TSL spectra of the undoped sample prepared from 4*N* Lu_2O_3 (un2) and of the Ce0.03 wt % doped one in four selected temperature regions are reported in Figs. 3(a) and 3(b), respectively. Below 70 K, the TSL spectrum of un2 is dominated by the Lu_{Al} antisite defect (AD)-related emission band within 3.5–4 eV. AD-related emission is well known from luminescence spectra of undoped YAG[19–21] and recently was reported also for the LuAG crystal.[22] The sharp line at about 2.02 eV and its few satellites can be ascribed to transitions from the $^5D_0$ level of Eu^{3+} impurities. By increasing the temperature above ~100 K, the AD-related emission becomes weaker while that of Eu^{3+} is noticeably strength-

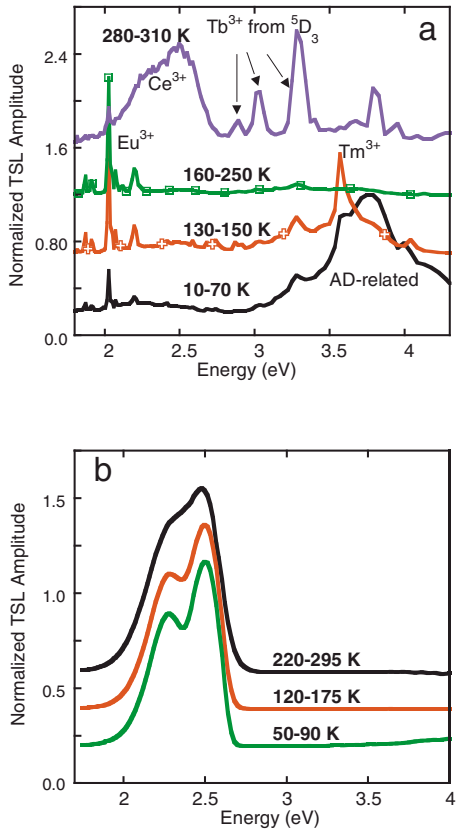

FIG. 3. (Color online) TSL spectra related to the glow curves reported in Fig. 1: (a) undoped (un2) sample and (b) 0.03 wt % Ce-doped sample. The spectra have been obtained by the integration of wavelength resolved measurements in the temperature intervals marked in the figure.

ened. Furthermore, also the emission at 3.56 eV from the $^1D_2$ level of Tm^{3+} impurity appears, see the curve labeled 130–150 K in Fig. 3(a). In the 160–250 K interval, the TSL spectrum is dominated by the mentioned Eu^{3+} emission. A complete change is noticed at temperatures above ~280 K since the TSL spectrum becomes dominated by emissions from Ce^{3+} and Tb^{3+} ions. Ce-doped samples show only the characteristic Ce^{3+} emission doublet peaking at 2.27 and 2.5 eV at any temperature, see Fig. 3(b).

The dose dependence of glow curves was investigated in Ce-doped samples within more than 2 orders of magnitude in order to examine the kinetic order of the glow peaks related to AD. So, this experiment was focused on the group of peaks in the 140–190 K range. In a first experiment when TSL measurements were performed up to RT, by increasing the dose, an anomalous shift of the peaks toward higher temperatures was noticed. Such effect cannot be explained by any specific kinetic recombination model within a single trap. Alternatively, one can suppose that it could be related to the presence of deeper traps (like those indeed observed above 200 K), which are close in space to those under investigation and cause carrier transfer by tunneling toward them, thus accelerating the detrapping rate of more shallow AD levels. So, we performed an alternative procedure aimed at investigating the dose dependence of 140–190 K peaks

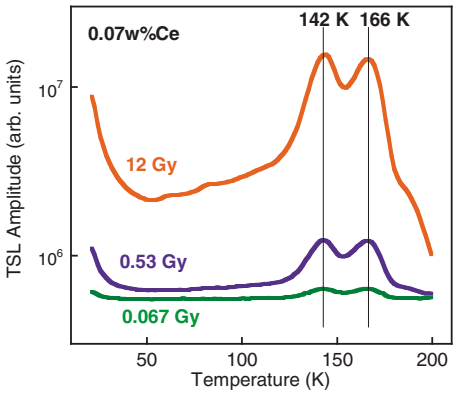

FIG. 4. (Color online) TSL glow curves of LuAG:0.07 wt % Ce at different irradiation doses marked in the legend. Curves are shifted on the ordinate scale for better clarity.

while keeping deep traps inactive by previous complete filling. Namely, x-ray irradiation was followed by a TSL run limited only to 200 K; moreover, the measurement sequence started with the highest dose (Fig. 4). In this case, the peak positions remained constant with increasing dose, which demonstrates that all the dominant peaks marked in Fig. 4 obey first order kinetics. The same experiment, performed up to 310 K, confirmed first order recombination kinetics also for the glow curve peaks at 237 and 280 K.

A deeper investigation of the TSL glow curve structure was performed by partial cleaning treatments and trap depth evaluation by the "initial rise" method as in our previous work on LuAG:Ce,Zr above RT.[23] This method consists of an x-ray irradiation of the sample, at 10 K in this case, followed by heating up to a partial cleaning temperature T_{stop}, and a further cooling afterward; finally, the glow curve is recorded. In this way, the initial portion of each peak composing the glow curve is measured without any contribution of the lower temperature peaks, and one can analyze it using a simple exponential function,[24]

$$I(T) = I_0 \exp[-E_T/kT], \tag{1}$$

where $I(T)$ is the TSL amplitude, E_T is the thermal depth, and k is the Boltzmann constant. Application of this method to TSL glow curve peaks within 120–200 K of the 0.03 wt % Ce sample yielded trap depth values of 0.31, 0.38, and 0.47 eV for the peaks at 142, 166, and 187 K, respectively. By applying the same procedure to the 237 and 280 K peaks, trap depth values of 0.57 and 0.48 eV were obtained, respectively. In Fig. 5, the glow curves after partial cleaning treatments are reported together with an example of exponential fit. Once the trap depth is known, according to the first order TSL process, the frequency factor s can be calculated using the simple equation

$$s = (\beta E/kT_m^2)\exp[E/kT_m], \tag{2}$$

while the detrapping times τ at any temperature T can be calculated as

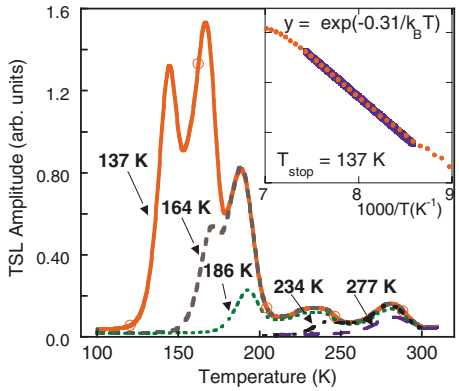

FIG. 5. (Color online) TSL glow curves of LuAG:0.03 wt % Ce after different partial cleaning steps at T_{stop} temperatures as marked in the figure. The inset displays an example of data exponential fit.

$$\tau = s^{-1} \exp[E/kT], \tag{3}$$

where E(eV) is the temperature of the peak, k is the Boltzmann constant, and β(K/s) is the temperature heating rate.

Trap depth, frequency factor, and detrapping time at RT are reported in Table I for all the investigated TSL peaks.

B. Phosphorescence decay

To clarify the origin of the broad structureless TSL signal below the edge of the 140 K peak, phosphorescence decays after x-ray irradiation at a constant temperature were measured in the 10–100 K range and in time intervals up to 1 h, as an extension of experiments reported by us recently.[17] Within all this temperature range, the decays are of closely similar shape (Fig. 6) and follow the formula

$$I(t) = A(t + t_0)^{-p}, \tag{4}$$

where $I(t)$ is the phosphorescence amplitude and A and t_0 are constants. The parameter p converges at any temperature to a value close to 1 and shows a slight temperature dependence (Fig. 7). Thus, the presence of a tunneling recombination mechanism as proposed in Ref. 17 and based on the model in Ref. 18 is firmly confirmed up to 100 K. Recent theoretical studies dealing with the explanation of power-decay law in luminescence justify the variation of such parameter within 0.95–1.5 values in the framework of the considered tunneling process between trapped electrons and randomly distributed recombination centers. Moreover, the slight increase of parameter p with temperature might indicate the presence of thermally assisted tunneling at higher temperatures.[25].

TABLE I. Parameters of TSL glow curve peaks evaluated in the case of LuAG:0.03 wt % Ce. The errors of trap depth values and detrapping times are approximately 3% and 10%, respectively. Approximate values of frequency factors are also reported.

TSL peak temperature (K)	Trap depth (eV)	Frequency factor (s^{-1})	Detrapping time at RT (s)
142	0.31	$\sim 10^9$	1.2×10^{-4}
166	0.38	$\sim 5\times10^9$	6.3×10^{-4}
187	0.47	$\sim 5\times10^{10}$	1.7×10^{-3}
237	0.57	$\sim 10^{10}$	4.0×10^{-1}
280	0.49	$\sim 5\times10^6$	5.6×10^{1}

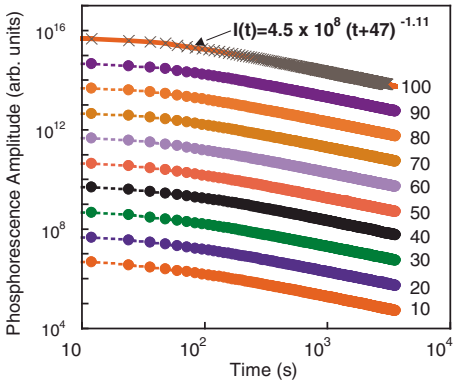

FIG. 6. (Color online) Phosphorescence decay at different temperatures marked in the figure after x-ray irradiation (irradiation dose=12 Gy). The decay obeys precisely the formula $I(t)=A\ (t+t_0)^{-p}$. An example of the fit is displayed for $T=100$ K by a solid line. Curves are shifted on the ordinate scale for better clarity.

The exact phosphorescence decay form observed within 10–100 K according to Eq. (4) confirms the presence of a tunneling mechanism and, at the same time, it also confirms the absence of any shallow trap with respect to that related to the glow curve peak at 142 K. In this respect, the structureless, nevertheless pronounced increase of TSL signal in the 0.12 wt % Ce sample above 50 K is difficult to understand under the assumption that in the trap, there is only a ground state level from which the trapped electron tunnels toward a hole localized at Ce^{4+}. A solution to this problem could consist in the existence of an excited state of the electron trap, from which electron tunneling occurs with higher probability with respect to ground state. Such situation has been reported in the TSL of other materials.[26] Thermally assisted tunneling processes were also considered in low temperature dielectric losses of crystalline quartz.[27] Qualitatively, one can propose a simple model limited to a single couple of electron and hole trapping sites at a specific distance r, see inset of Fig. 8. In the electron trap, there is a ground (0) and an excited (1) state separated by an energy E_1, and the probabilities of tun-

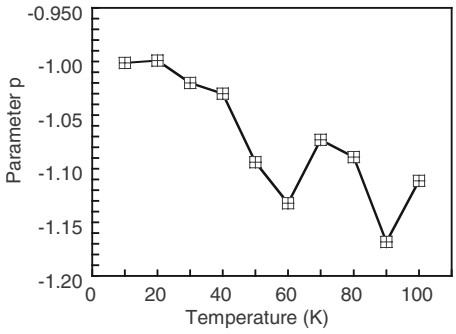

FIG. 7. Temperature dependence of parameter p of Eq. (4).

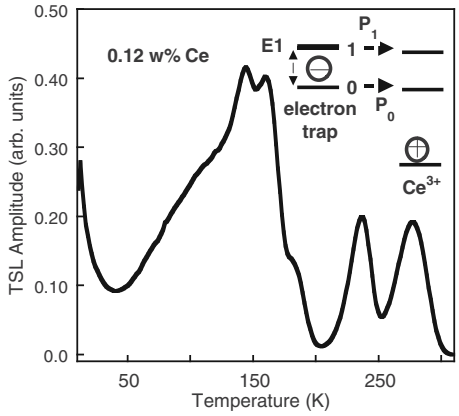

FIG. 8. TSL glow curve of LuAG:0.12 wt % Ce after x-ray irradiation at 10 K. X-ray dose=10 Gy. In the inset, there is a sketch of thermally stimulated tunneling process between an adjacent electron trap and Ce^{3+} recombination center.

neling toward the Ce^{3+} excited state from the trap ground and excited states are P_0 and P_1, respectively. If we consider $P_1 > P_0$, accelerated tunneling via excited state 1 will explain the increasing TSL intensity within 50–120 K and the increasing value of parameter p with temperature as well (Fig. 7). It is also interesting to note that up to 20–25 K, the dependence of the TSL glow curve amplitude well follows a T^{-1} dependence, i.e., it is similar to that found in the phosphorescence decays in Fig. 6 (taking into account that a linear heating rate of 0.1 K/s is adopted, i.e., that time t and temperature T are in a linear relation). This can be explained under the assumption that at low temperatures before a significant population of excited state 1 of the trap is achieved, electrons tunnel only from the ground state level (0) and macroscopic averaging over the ensemble of all electron-hole tunneling species brings to a t^{-1} (i.e., T^{-1} due to the linear heating rate) dependence, as that observed in isothermal phosphorescence decays.

C. Scintillation decay

Scintillation decay of LuAG:Ce is characterized by a two-stage course consisting of a leading component with decay time comparable to the photoluminescence one (~54 ns at RT) and a slower process usually approximated by a second exponential with several hundreds of nanoseconds decay time.[17] It appears difficult to attribute a physical meaning to this slower decay process since the detrapping times related to TSL peaks are of the order of 100 μs or longer. Taking into account the presence of tunneling recombination evidenced in phosphorescence decay measurements in Sec. III B, it is worth to attempt a fit of scintillation decay by the sum of exponential and power functions, namely,

$$I(t) = A \exp[-t/\tau] + B(t - t_0)^{-p} + C, \tag{5}$$

where A, B, and t_0 are constants and C is the experimental background. The exponential and power function components account for the first and second stages of the scintillation decay, respectively. The result is displayed in Fig. 9,

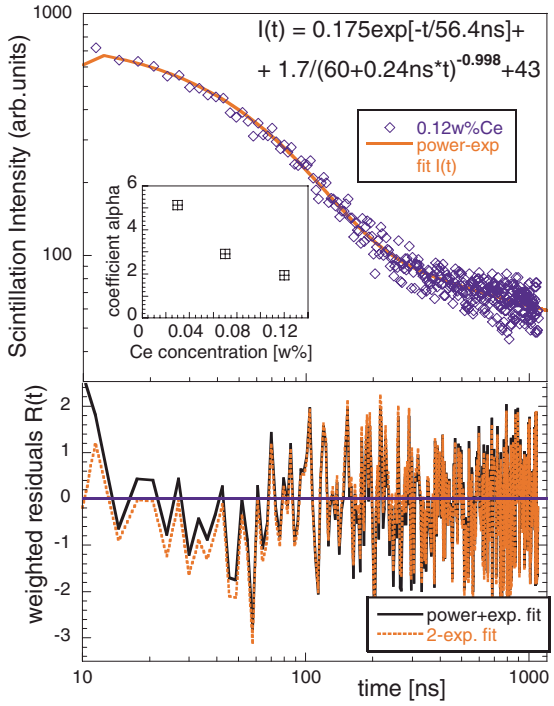

FIG. 9. (Color online) Spectrally unresolved scintillation decay of LuAG:0.12 wt % Ce at RT. Red solid line is the data reconstruction using an exponential+power function [Eq. (4)]; weighted residuals of the fit are presented in the bottom part of the graph for both the $I(t)$ fitting function reported in the figure and for the two-exponential approximation $I_2(t) = 626 \exp[-t/59\ \text{ns}] + 54 \exp[-t/958\ \text{ns}] + 43$.

where the solid line is the convolution of the instrumental response and function $I(t)$ according to Eq. (5). An excellent fit is obtained, which gives a decay time (τ) value even closer to the photoluminescence one and shows more symmetric residuals with respect to the common two-exponential approximation reported in the caption of Fig. 9. The value of parameter p converges very close to 1, supporting the presence of a thermally assisted tunneling mechanism at RT even in the submicrosecond time scale. It is worth noting that a t^{-1} decay law was observed also in other materials down to tens of nanosecond time scale.[25]

In scintillation measurements, the presence of very slow decay processes of the order of tens to hundreds of microseconds can be evidenced also from the increased signal level before the rising edge of scintillation decay. It can be quantitatively evaluated by a parameter α, as the percentage ratio between such superslow component amplitude (I_{ss}) and the total decay amplitude I_{tot}, $\alpha = 100 \times I_{ss}/I_{tot}$, see also Refs. 7 and 17. Such decay times are comparable to RT detrapping times of TSL peaks in the 140–190 K region. A correlation between the coefficient α and the amplitude of TSL peaks is found since they both decrease with increasing cerium concentration, as reported in the inset of Fig. 9 (coefficient α) and in Fig. 2(b) (the 140 K peak).

D. Electron paramagnetic resonance

EPR experiments performed on the same samples revealed several inequivalent Ce^{3+} centers. From the analysis

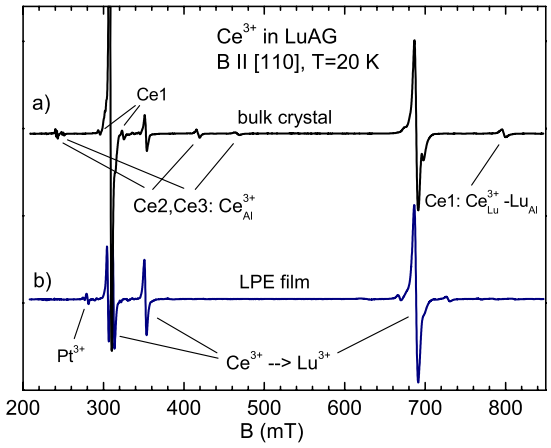

FIG. 10. (Color online) Ce^{3+} EPR spectra of (a) LuAG:0.03 wt % Ce bulk crystal and (b) LPE single crystalline film (~0.5 wt % Ce). Main Ce^{3+} spectrum corresponds to Ce^{3+} at Lu lattice sites, while other (Ce1, Ce2, and Ce3) spectra correspond to Ce^{3+} at perturbed Lu and Al sites, respectively. The small splitting of the resonance line at $B=312$ mT in the LPE film is caused by the small tilting of its plane from the (110) crystal plane.

of the angular dependencies of the EPR spectra, three types of structurally inequivalent sites for the Ce^{3+} ions in the LuAG lattice were distinguished, in addition to the regular Ce^{3+}_{Lu} one [Fig. 10, curve (a); for details, see Ref. 28]. The first one (denoted Ce1) is related to Ce^{3+} ions in the normal Lu position, which is, however, perturbed by a defect located at one of the neighboring Al sites. At least six such magnetically inequivalent Ce^{3+} sites can be distinguished from the measured spectra in (110) and (100) planes. Their spectrum is described by the orthorhombic symmetry g tensor with the following components: $g_1=2.030(1)$, $g_2=0.780(1)$, and $g_3=2.580(1)$, where two of the principal axes are tilted from the $\langle 110\rangle$ directions by the angle of $\pm 8.5°$ [Euler angles: $\alpha=(45\pm 8.5)°$, $\beta=0$, and $\gamma=0$]. The relative concentration of Ce1 centers is approximately 3%–6% of the total Ce^{3+} content and does not depend on the Ce concentration (at least up to 0.07 wt % Ce doping level) or purity of the crystals. At the same time, Ce1 centers are not observed in LPE-grown single crystalline films [Fig. 10, curve (b)], the preparation temperature of which is well below 1000 °C that hinders AD creation.[10,28] Thus, the perturbation can hardly be related to accidental cationic impurities in the crystal, the total amount of which is less then a few tens of ppm. It is suggested that the perturbation comes from a Lu ion at the antisite octahedral position. So, Ce^{3+} ions and Lu_{Al} antisite defects can be spatially correlated. Two other Ce^{3+} centers (denoted as Ce2 and Ce3) are most probably created by Ce^{3+} ions at distorted Al octahedral sites. It follows from the fact that the largest distortion in Ce2 and Ce3 centers occurs at directions close to the $\langle 111\rangle$ axes that have to be for an impurity placed at distorted octahedral sites. There are eight such magnetically inequivalent positions of the Ce^{3+} in the centers Ce2 and Ce3, and spectral parameters of these centers are given in Ref. 28. The relative concentration of this type of Ce centers is also around 3%–4% and does not depend on the Ce concentration. We should note that the ionic radius of Ce^{3+} at the octahedral position (1.15 Å) (Ref. 29) is markedly larger than that of Al^{3+} (0.675 Å). However, the presence of an oxygen vacancy near the Ce^{3+} ion can reduce the ionic radius of Ce^{3+} to the value comparable to the ionic radius of Lu^{3+}(Al) in regular octahedron due to a decreasing coordination number. Oxygen vacancy can also provide more space for Ce location at the octahedral site. Alternatively, the Ce2 and Ce3 centers could be ascribed also to perturbed Lu dodecahedral sites. However, in our opinion, this ascription is not well supported by both the principal axis orientation and g-factor values found from the experiment.

IV. DISCUSSION

TSL spectra reported in Figs. 3(a) and 3(b) provide information about the mechanism of charge carrier localization and thermal detrapping in LuAG host. The ADs were identified as shallow electron traps both in YAG[9] and LuAG[10,30] hosts. Eu ion is also evidenced both in YAG and LuAG in the stable 3+ charge state from its photoluminescence spectra[31,32] so that it can act only as an electron trap due to its easy switch to the 2+ charge state. The same consideration holds for Tm ion too.[33] On the contrary, both Ce and Tb ions are well evidenced in aluminum garnets in stable trivalent state but can easily exist also in the 4+ charge state, so that these ions act as hole traps in LuAG lattice. At 10 K, during x-ray irradiation, free holes are localized at unknown sites of the lattice and at accidental impurities such as Ce^{3+} and Tb^{3+} ions, while electrons are trapped at AD Lu_{Al} defects, Eu^{3+} and Tm^{3+} ions, and probably also at other unknown lattice defects. TSL spectra point to the fact that in undoped samples below 280 K, holes are thermally freed from various traps, so hole traps determine TSL peak positions. They undergo recombination with electrons localized at AD, Eu and Tm ions, which are responsible for the observed TSL spectra. Remaining electrons trapped at AD defects are gradually thermally freed above 120 K.[10] It results in their retrapping at Eu and Tm impurity ions, which is reflected in the strong increase of related emission line amplitudes in the 130–250 K range [Fig. 3(a)]. The complete change of the TSL emission pattern above 280 K points to the thermal emptying of electron traps and recombination of free electrons with holes trapped at Ce and Tb ions. In Ce-doped samples, during x-ray irradiation at 10 K, the major part of the holes becomes localized at Ce^{3+} ions, so that the TSL glow curve is entirely determined by the characteristics of available electron traps dominated by AD defects,[10] while TSL emission spectra show only the Ce^{3+} emission band.

To our knowledge, there are no reports in the literature which evidence trapped or self-trapped holes in YAG or LuAG crystals by EPR. However, the small concentration of Ce^{3+} ions (0.07 wt % Ce) sufficient to completely suppress the undoped sample TSL pattern, the variability of the glow curve shape in undoped samples, and their much weaker TSL signal amplitudes with respect to the Ce-doped ones point to defect-bound hole centers. Consequently, there is no analogous hole self-trapping process as that occurring in aluminum perovskites, giving rise to intense TSL peaks within 150–250 K (Refs. 17 and 34).

The electron traps related to the 237 and 280 K peaks also deserve some comment. These peaks are commonly found in LuAG:Ce (Refs. 5 and 23) and their amplitudes increase with the Ce concentration [Fig. 2(b)]. Their dose dependence points to a first order process. The frequency factor s of the 280 K peak shows markedly lower values with respect to those of other TSL peaks (Table I), suggesting a tight space correlation between the responsible electron trap and Ce^{3+} ion.

Detrapping times at RT calculated for all the TSL peaks (see Table I) are longer than 100 μs, so that thermal emptying of these traps and conduction-band-mediated recombination mechanism cannot explain the submicrosecond slower decay component in the scintillation response. Instead, it seems that correlation between the 140 K TSL peak (detrapping time ~0.1 ms) and the coefficient α value in the scintillation decay can be well explained considering thermally induced electron detrapping into conduction band followed by the delayed electron-hole recombination at Ce^{3+} centers.

The broad and structureless TSL signal well evident below ~120 K in Ce-doped samples is due to a tunneling process between electrons captured at antisite Lu_{Al} defects and holes localized at Ce ions. As the Ce concentration increases, the mean distance in the Ce-Lu_{Al} pairs is shortened and this favors the tunneling mechanism with respect to the thermally induced conduction-band-mediated recombination process. This is well reflected in the Ce-concentration dependence of the TSL glow curve pattern below 200 K. Thermally assisted tunneling from an excited state in the trap can explain the TSL amplitude gradual increase within 50–120 K in the highest Ce-concentration sample. Moreover, EPR experiments suggest the presence of a Lu_{Al} AD in the vicinity of Ce^{3+} ions. Based on these results, we propose that the slow submicrosecond component in the scintillation decay at RT arises due to the mentioned thermally assisted tunneling process. Supporting arguments are obtained from numerical analysis of the scintillation decay, where the fit using a combination of exponential and inverse power function appears to be slightly more accurate with respect to the classical two-exponential approximation. It is also worth noting that in single crystalline LuAG:Ce layers prepared by LPE, no perturbation of Ce^{3+} EPR-active centers was found and the amplitude of a slow submicrosecond decay component under above-band-gap excitation is also lower with respect to bulk single crystals.[35] Unfortunately, EPR experiments did not reveal any hole centers related to the LuAG lattice itself so far, so that the nature of hole traps responsible for TSL glow curve peaks below 280 K in undoped samples remains an open question. However, suggested spatial correlation between Ce^{3+} ions and Lu_{Al} antisite defects is of crucial importance to explain both the TSL and scintillation decay characteristics discussed above.

V. CONCLUSIONS

This study, involving TSL, phosphorescence, scintillation, and EPR measurements, reveals the presence of tunneling phenomena in radiative recombination processes of LuAG:Ce single crystals. They involve shallow electron traps and Ce^{3+} ions as the recombination centers. The former are due to antisite Lu_{Al} centers, which should be typical defects in the high temperature melt-grown bulk single crystals.

TSL spectra of undoped samples suggest that up to 280 K, holes are freed from several different host lattice-related traps and they are responsible for the observed glow curve pattern. On the contrary, in the Ce-doped material, the majority of the holes is trapped at Ce^{3+} ions and the glow curve pattern is dominated by the electron release from Lu_{Al} defect-related traps. In Ce-doped samples, the first order process in the TSL mechanism has been verified by the dose dependence of the TSL signals over more than 2 orders of magnitude. From partial cleaning treatments, the trap depths related to five characteristic TSL peaks were calculated using the initial rise method.

In the 10–100 K range, the phosphorescence decays at constant temperature following x-ray irradiation obey the t^{-1} law in perfect agreement with theoretical models describing the tunneling-driven radiative carrier recombination. At RT, the slow submicrosecond component in the scintillation decay follows a t^{-1} form as well and can be interpreted as due to the thermally assisted tunneling-driven radiative recombination, too. This interpretation provides a physical ground for the submicrosecond-scale recombination decay processes in LuAG:Ce scintillator contrary to the common multiexponential analysis, which cannot be justified using calculated detrapping times at RT from the identified shallow electron traps.

EPR experiments verified the existence of Ce^{3+} centers featuring a perturbation at one of the nearest aluminum sites. The relatively high concentration of perturbers and the elevated purity of the crystals point to the Lu_{Al} defects as the most probable perturber. The occurrence of Lu_{Al} defects in the vicinity of Ce^{3+} ions provides strong support to the existence of tunneling phenomena in radiative recombination processes.

ACKNOWLEDGMENTS

Financial support of Czech Projects GA AV No. S100100506, MSMT No. 1M06002 and Italian project of Cariplo Foundation 2006–2008 "Structure and optical properties of self-organized nano- and mesoscopic materials" is gratefully acknowledged. Thanks are due to Yu. Zorenko for providing us the LPE samples for EPR experiment.

[1] C. D. Brandle, J. Cryst. Growth **264**, 593 (2004).
[2] R. Autrata, P. Schauer, Jos. Kvapil, and J. Kvapil, J. Phys. E **11**, 707 (1978).
[3] M. Moszynski, T. Ludziewski, D. Wolski, W. Klamra, and L. O. Norlin, Nucl. Instrum. Methods Phys. Res. A **345**, 461 (1994).
[4] A. Lempicki, M. H. Randles, D. Wisniewski, M. Balcerzyk, C. Brecher, and A. J. Wojtowitz, IEEE Trans. Nucl. Sci. **42**, 280 (1995).
[5] M. Nikl, E. Mihokova, J. A. Mares, A. Vedda, M. Martini, K. Nejezchleb, and K. Blazek, Phys. Status Solidi B **181**, R10 (2000).
[6] K. Blazek, A. Krasnikov, K. Nejezchleb, M. Nikl, T. Savikhina, and S. Zazubovich, Phys. Status Solidi B **241**, 1134 (2004).
[7] M. Nikl, Phys. Status Solidi A **202**, 201 (2005).
[8] J. A. Mares, A. Beitlerova, M. Nikl, N. Solovieva, C. D'Ambrosio, K. Blazek, P. Maly, K. Nejezchleb, and F. de Notaristefani, Radiat. Meas. **38**, 353 (2004).
[9] E. Mihóková, M. Nikl, J. A. Mareš, A. Beitlerová, A. Vedda, K. Nejezchleb, K. Blažek, and C. D'Ambrosio, J. Lumin. **126**, 77 (2007).
[10] M. Nikl, E. Mihokova, J. Pejchal, A. Vedda, Yu. Zorenko, and K. Nejezchleb, Phys. Status Solidi B **242**, R119 (2005).
[11] Yong-Nian Xu and W. Y. Ching, Phys. Rev. B **59**, 10530 (1999).
[12] M. G. Shelyapina, V. S. Kasperovich, and P. Wolfers, J. Phys. Chem. Solids **67**, 720 (2006).
[13] M. M. Kuklja, J. Phys.: Condens. Matter **12**, 2953 (2000).
[14] C. R. Stanek, K. J. McClellan, M. R. Levy, and R. W. Grimes, Phys. Status Solidi B **243**, R75 (2006).
[15] M. Kh. Ashurov, Yu. K. Voronko, V. V. Osiko, A. A. Sobel, and M. I. Timoshechkin, Phys. Status Solidi A **42**, 101 (1977).
[16] V. Lupei, A. Lupei, C. Tiseanu, S. Georgescu, C. Stoicescu, and P. M. Nanau, Phys. Rev. B **51**, 8 (1995).
[17] M. Nikl, V. V. Laguta, and A. Vedda, Phys. Status Solidi A **204**, 683 (2007).
[18] P. Avouris and T. N. Morgan, J. Chem. Phys. **74**, 4347 (1981).
[19] D. J. Robbins, B. Cockayne, J. L. Glasper, B. Lent, J. Electrochem. Soc. **126**, 1213 (1979).
[20] L. G. Volzhenskaya, Yu. V. Zorenko, N. I. Patsagan, and M. V. Pashkovsky, Opt. Spectrosc. **63**, 790 (1987).
[21] V. Mürk and N. Yaroshevich, J. Phys.: Condens. Matter **7**, 5857 (1995).
[22] V. Babin, K. Blazek, A. Krasnikov, K. Nejezchleb, M. Nikl, T. Savikhina, and S. Zazubovich, Phys. Status Solidi C **2**, 97 (2005).
[23] A. Vedda, D. Di Martino, M. Martini, V. V. Laguta, M. Nikl, E. Mihokova, J. Rosa, K. Nejezchleb, and K. Blazek, Phys. Status Solidi A **195**, R1 (2003).
[24] S. W. S. Mc Keever, *Thermoluminescence of Solids* (Cambridge University Press, Cambridge, 1985).
[25] D. J. Huntley, J. Phys.: Condens. Matter **18**, 1359 (2006).
[26] I. F. Chang and P. Thioulouse, J. Appl. Phys. **53**, 5873 (1982).
[27] W. J. de Vos and J. Volger, Physica (Amsterdam) **47**, 13 (1970).
[28] V. V. Laguta, A. M. Slipenyuk, M. D. Glinchuk, I. P. Bykov, Yu. Zorenko, M. Nikl, J. Rosa, and K. Nejezchleb, Radiat. Meas. **42**, 835 (2007).
[29] R. D. Shannon, Acta Crystallogr., Sect. A: Cryst. Phys., Diffr., Theor. Gen. Crystallogr. **32**, 751 (1976).
[30] M. Nikl, J. Pejchal, E. Mihokova, J. A. Mares, H. Ogino, A. Yoshikawa, T. Fukuda, A. Vedda and C. D'Ambrosio, Appl. Phys. Lett. **88**, 141916 (2006).
[31] M. S. Scholl and J. R. Trimmer, J. Electrochem. Soc. **133**, 643 (1986).
[32] Z. Wang, M. Xu, W. Zhang, and M. Yin, J. Lumin. **122-123**, 437 (2007).
[33] G. Armagan, B. Di Bartolo, and A. M. Buoncristiani, J. Lumin. **44**, 141 (1989).
[34] O. F. Schirmer, K. W. Blazey, and W. Berlinger, Phys. Rev. B **11**, 4201 (1975).
[35] Yu. Zorenko, V. Gorbenko, A. Voloshinovskii, G. Stryganyuk, V. Mikhailin, V. Kolobanov, D. Spassky, M. Nikl, and K. Blazek, Phys. Status Solidi A **202** 1113 (2005).